The Astrophysical Journal, 653:756–764, 2006 December 10

ANGULAR MOMENTUM TRANSPORT BY GRAVITY WAVES IN THE SOLAR INTERIOR

Tamara M. Rogers
Astronomy and Astrophysics Department, University of California, 1156 High Street, Santa Cruz, CA 95064; trogers@pmc.ucsc.edu

and

Gary A. Glatzmaier
Earth Sciences Department, University of California, Santa Cruz, CA 95064
Received 2005 November 21; accepted 2006 June 13

ABSTRACT

We present self-consistent numerical simulations of the Sun's convection zone and radiative interior using a two-dimensional model of the solar equatorial plane. The background reference state is a one-dimensional solar structure model. Turbulent convection in the outer convection zone continually excites gravity waves that propagate throughout the stable radiative interior and deposit their angular momentum. We find that angular velocity variations in the tachocline are driven by angular momentum transported by overshooting convective plumes rather than nonlinear interaction of waves. The mean flow in the tachocline is time dependent but not oscillatory in direction and not like a quasi-biennial oscillation (QBO). Since the forcing in this shallow region cannot be described by simple linear waves, it is unlikely that the interaction of such waves is responsible for the solar cycle or the 1.3 yr oscillation. However, in the deep radiative interior, the interaction of low-amplitude gravity waves, continually excited by the overshooting plumes, is responsible for the angular velocity deviations observed there, which do resemble a very low amplitude QBO. Near the center of the model Sun the angular velocity deviation is about 2 orders of magnitude greater than that in the bulk of the radiative region and reverses its direction (prograde to retrograde or vice versa) in the opposite sense of the angular velocity deviations that occur in the tachocline. Our simulations thus demonstrate how angular velocity variations in the solar core are linked to those in the tachocline, which themselves are driven by convective overshooting.

Subject headings: convection — Sun: interior

1. INTRODUCTION

Internal gravity waves are ubiquitous in nature. Their influence can be observed in striated cloud structures in our own atmosphere many days of the year. In addition to the visual display of these waves in our atmosphere, they have other more profound consequences. The interaction of gravity waves with angular velocity shear produces the quasi-biennial oscillation (QBO), which dominates variability in the equatorial stratosphere and affects ozone levels.

Gravity waves have been invoked to explain several physical problems in stellar interiors, such as (1) providing the extra mixing required to solve the Li depletion problem in F stars (Garcia-Lopez & Spruit 1991) and in the Sun (Montalban 1994), (2) increasing turbulent mixing and affecting the solar neutrino production (Press 1981), (3) maintaining the solid body rotation of the Sun's radiative interior (Schatzman 1993; Zahn et al.1997; Kumar & Quataert 1997), and (4) controlling the solar cycle (Kumar et al.1999, hereafter KTZ99). Internal gravity waves have also been studied in binary stars (Zahn 1975; Goldreich & Nicholson 1989) and have been used to explain the orbital properties of those star systems (Terquem et al. 1998). These theories, however, are only as good as the poorly understood excitation and evolution of gravity waves in stellar interiors. What gravity wave spectra and amplitudes are generated? How effectively do gravity waves transport angular momentum and mix species?

Some confusion has existed. For example, although gravity waves were postulated to extract angular momentum from the solar radiative interior and so enforce solid body rotation (Zahn et al.1997; Schatzman 1993; Kumar & Quataert 1997), it was quickly pointed out (Gough & McIntyre 1998; Ringot 1998) that gravity waves tend to enhance local shear rather than smooth it.

Recognizing this antidiffusive nature of gravity waves in shear flows, several authors published papers postulating an angular velocity oscillation at the base of the solar convection zone analogous to the QBO in the Earth's stratosphere (Baldwin et al. 2001). In KTZ99, a spectrum of gravity waves generated by the overlying convection is prescribed (adapted from Goldreich et al. 1994). This spectrum is then integrated to give a flux of angular momentum that is transferred from the waves to the mean flow, resulting in a periodic oscillation of angular velocity at the base of the convection zone with a timescale of about 20 yr. In another paper (Kim & MacGregor 2001) a two wave model is assumed: one prograde propagating wave with a prescribed angular momentum flux, and one retrograde wave with another (negative) prescribed flux. In addition, these authors include viscous dissipation in the evolution equation for the mean flow and find that the nature of the resulting angular velocity oscillation depends sensitively on the value of the assumed viscous diffusivity. For large viscous diffusivity a steady solution is found, whereas for small values a chaotic oscillation is found. A periodic solution is recovered only for intermediate values of the viscous diffusivity.

More recently, the KTZ99 model has been extended to show that the oscillating shear layer at the base of the convection zone acts as a filter on the low-frequency short-wavelength waves (Talon et al. 2002; Talon & Charbonnel 2005). In their theory, the filter preferentially damps prograde waves, allowing predominantly retrograde waves, which carry negative angular momentum, into the deep interior. When these waves dissipate they transfer their negative angular momentum to the flow, and therefore effectively extract prograde angular momentum from the low-latitude, deep-solar interior, leading to solid body rotation in the solar radiative zone.

The major shortcoming of both of these models is twofold. First, neither model self-consistently calculates the generation of the gravity waves by the solar convection zone. In KTZ99 a spectrum and amplitude of gravity waves is assumed, a spectrum

that is unfortunately untestable with observations and has not been reproduced in numerical simulations. In addition, this spectrum neglects the production of gravity waves by overshooting plumes. Second, and perhaps more importantly, neither model calculates the nonlinear wave-wave interactions (Reynolds stresses), which contribute to the mean flow (see eq. [1], first term on right hand side). In the past this nonlinear interaction has been prescribed as a flux that is a function of height (KTZ99 and subsequent papers; Kim & MacGregor 2001); in the present work we self-consistently and explicitly calculate this nonlinear interaction rather than parameterizing it.

Here we present numerical simulations that address both of these issues. Our model solves the fully nonlinear Navier-Stokes equations in both the convective and radiative regions. Therefore, the gravity waves are self-consistently generated by an overlying convection zone, and the nonlinear terms are retained in the radiation zone to account for the nonlinear wave interactions that affect the mean flow.

2. WAVE-SHEAR FLOW INTERACTIONS

In this section we briefly review the hydrodynamic process by which waves can transport their angular momentum to the flow in which they travel. The natural example of this process is the QBO. For a more complete discussion of the QBO see, e.g., Baldwin et al. (2001), Lindzen (1990), and Holton (1994).

For simplicity consider the Boussinesq equations for a viscous fluid in two-dimensional Cartesian (x-z) coordinates, x being the horizontal coordinate and z the vertical coordinate. After decomposing the horizontal velocity into mean flow ($\overline{U}$, a function of z) and fluctuating (u') components and taking the proper horizontal average, the equation for the mean horizontal velocity becomes

$$\frac{\partial \overline{U}}{\partial t} = -\frac{\partial \overline{u'w'}}{\partial z} + \nu \frac{\partial^2 \overline{U}}{\partial^2 z}. \tag{1}$$

In equation (1), u' represents the fluctuating horizontal velocity and w' represents the fluctuating vertical velocity. This simple equation represents how small scale wave-wave interactions (Reynolds stresses) influence the mean flow ($\overline{U}$). The only way a nonaxisymmetric wave can transport angular momentum to the axisymmetric mean flow is by a nonlinear interaction, i.e., the convergence of the $\overline{u'w'}$ flux, which requires wave attenuation (such as radiative damping or critical layers).

In the presence of differential rotation the picture becomes more complicated. In a rotating fluid, waves generated at a particular frequency are Doppler-shifted away from that frequency according to the equation

$$\omega(r) = \omega_{\rm gen} + m\left[\Omega_{\rm gen} - \Omega(r)\right], \tag{2}$$

where m is the horizontal wavenumber, $\omega_{\rm gen}$ is the frequency at which the wave is generated in the frame rotating at $\Omega_{\rm gen}$, and $\omega(r)$ is the frequency measured relative to the local rotation rate $\Omega(r)$.

Where $\Omega(r) > \Omega_{\rm gen}$ prograde waves ($m > 0$) are shifted to lower frequencies, and retrograde waves ($m < 0$) are shifted to higher frequencies. Since radiative damping is strongly frequency dependent (damping length $\propto \omega^4$), prograde (lower frequency) waves are damped in a shorter distance than retrograde (higher frequency) waves. This differential damping causes prograde waves to deposit their (positive) angular momentum closer to the generation site than retrograde waves deposit their (negative) angular momentum, thus leading to a double-peaked shear layer. As prograde (retrograde) waves continually deposit their positive (negative) angular momentum, the amplitude of the angular velocity shear increases. This increased shear causes prograde waves to be shifted to ever smaller frequencies that are damped even closer to the generation site. In this way the peak in the prograde layer moves toward the source of the waves. When the prograde shear becomes sufficiently steep it is broken down by viscous diffusion leaving behind the retrograde layer. This process repeats, with the period of the process inversely proportional to the wave forcing. The prominent features of this physical process are then threefold: (1) prograde flow lies above retrograde motion (or vice versa), i.e., a double-peaked shear, (2) this pattern propagates toward the generation site, and (3) the oscillation period is distinct from the forcing timescale.

This physical picture was proposed initially by Lindzen & Holton (1968) and Holton & Lindzen (1972) to explain the QBO observed in the Earth's atmosphere. Later, the physical theory was tested in the remarkable experiment by Plumb & McEwan (1978), and the basic physical mechanism was recovered. It has also been suggested that an oscillation similar to the QBO occurs in Jupiter's atmosphere (Leovy et al. 1991), coined the quasi-quadrennial oscillation (QQO) because of its 4 year period.

The robustness of this mechanism led astronomers to hypothesize that the same physical mechanism could be operating in the solar tachocline (KTZ99; Kim & MacGregor 2001; Talon & Charbonnel 2005). This could then provide a handsome explanation for oscillations at the base of the convection zone, whether on 20 yr timescales (as in the dynamo, KTZ99) or 1 yr timescales (as in the 1.3 yr oscillation, Kim & MacGregor 2001). We review this mechanism here, so that comparisons between this process and the zonal flow oscillations seen in the radiative region of our model can be clearly made.

3. NUMERICAL MODEL

The numerical technique and model setup are identical to those in Rogers & Glatzmaier (2005), except here we impose the equatorial rotation profile as a function of radius as inferred from helioseismology [$\Omega(r)$ is specified to be 465 nHz in the convection zone, 435 nHz in the stable region, and the tachocline is fit to an error function]. We solve the Navier-Stokes equations with rotation in the anelastic approximation in two-dimensional (2D) cylindrical geometry (r, θ). The curl of the momentum equation, i.e., vorticity equation, is

$$\frac{\partial \omega}{\partial t} + (\boldsymbol{v}\cdot\nabla)\omega = [2\Omega(r) + \omega]h_\rho v_r - 2v_r \frac{\partial \Omega(r)}{\partial r} - \frac{\overline{g}}{\overline{T}r}\frac{\partial T}{\partial \theta} - \frac{1}{\overline{\rho}\overline{T}r}\frac{\partial \overline{T}}{\partial r}\frac{\partial p}{\partial \theta} + \overline{\nu}\nabla^2\omega. \tag{3}$$

The heat equation is

$$\frac{\partial T}{\partial t} + (\boldsymbol{v}\cdot\nabla)T = -v_r\left[\frac{\partial \overline{T}}{\partial r} - (\gamma-1)\overline{T}h_\rho\right] + (\gamma-1)Th_\rho v_r + \gamma\overline{\kappa}\left[\nabla^2 T + (h_\rho + h_\kappa)\frac{\partial T}{\partial r}\right] + \gamma\overline{\kappa}\left[\nabla^2\overline{T} + (h_\rho + h_\kappa)\frac{\partial \overline{T}}{\partial r}\right] + \frac{\overline{Q}}{c_v}. \tag{4}$$

In these equations, $\boldsymbol{v}$ is the velocity, with radial, $\boldsymbol{v}_r$, and longitudinal, $\boldsymbol{v}_\theta$, components. The vorticity is $\boldsymbol{\omega} = \nabla \times \boldsymbol{v}$ and is normal to the equatorial plane in this 2D geometry. The functions $h_\rho = d\ln\overline{\rho}/dr$, $h_\kappa = d\ln\overline{\kappa}/dr$, $\overline{g}$ (gravity), $\overline{T}$ (temperature), $\overline{\rho}$ (density), and γ (ratio of specific heats, c_p/c_v) are radially

dependent and taken from a standard solar model (J. Christensen-Dalsgaard 2006, private communication); T is the temperature perturbation and p is the pressure perturbation, which like ω, are functions of r, θ, and time (t). Note in equation (4) that

$$\frac{\partial \overline{T}}{\partial r} - (\gamma - 1)\overline{T} h_\rho \approx -\frac{\overline{g}}{R}(\nabla - \nabla_{\rm ad}), \quad (5)$$

where R is the gas constant.

In our model we specify the thermal diffusivity as that given by the solar model multiplied by a constant for numerical stability

$$\overline{\kappa} = k_m \frac{16\sigma \overline{T}^3}{3\overline{\rho}^2 \overline{k} c_p}. \quad (6)$$

Here k_m is generally set to 10^5, σ is the Stefan-Boltzman constant, and $\overline{k}$ is the opacity. The viscous diffusivity $\overline{\nu} = \mu/\overline{\rho}$, is set so that the dynamic viscosity (μ) is constant (10^{11} g cm^{-1} s^{-1}). These values for the diffusivities give a Rayleigh number ($=\overline{g}\alpha\,\Delta\nabla T D^4/\overline{\nu\kappa}$) that varies from 10^8 at the base of the convection zone to 10^7 at the top of the convection zone. Similarly, the Prandtl number varies from 10^{-3} in the radiative core to 10^{-2} at the top of the convection zone. The viscous diffusivity varies from 10^9 cm^2 s^{-1} in the radiative core to 10^{13} cm^2 s^{-1} at the top of the convection zone, while the thermal diffusivity varies from 10^9 cm^2 s^{-1} at the solar core to 10^{12} cm^2 s^{-1} at the base of the convection zone, where it subsequently drops again with radius (the same variation in height as the standard solar model). As in all solar convection simulations, these large viscous and thermal diffusivities are considered turbulent diffusivities representing the transport and mixing done by the unresolved (subgrid scale) motions.

We calculate the pressure term in (3) using the longitudinal component of the momentum equation

$$\frac{1}{\overline{\rho} r}\frac{\partial p}{\partial \theta} = -\frac{\partial v_\theta}{\partial t} - (\boldsymbol{v}\cdot\nabla\boldsymbol{v})_\theta + \overline{\nu}\left[(\nabla^2\boldsymbol{v})_\theta - \frac{h_\rho}{3r}\frac{\partial v_r}{\partial \theta}\right]. \quad (7)$$

These equations are supplemented by the continuity equation in the anelastic approximation

$$\nabla\cdot\overline{\rho}\boldsymbol{v} = 0 \quad (8)$$

that is satisfied by expressing $\overline{\rho}\boldsymbol{v}$ as the curl of a stream function. The model extends from 0.001 to 0.93 $R_\odot$. The subadiabaticity ($\nabla - \nabla_{\rm ad}$) in the radiative region is given by the solar model, and we specify the superadiabaticity in the convection zone to be 10^{-7}.

These equations are solved using a Fourier spectral transform method in the longitudinal (θ) direction and a finite difference scheme on a nonuniform grid in the radial (r) direction. Time advancing is done using the explicit Adams-Bashforth method for the nonlinear terms and an implicit Crank-Nicolson scheme for the linear terms. The boundaries are impermeable and stress free. The inner boundary is isothermal and the outer boundary is held at a constant heat flux. This code is parallelized using message passing interface (MPI) and the resolution is 2048 longitudinal zones × 1500 radial zones, with 620 radial zones dedicated to the radiative region. In the region just below the convection zone the radial resolution is 170 km. This model was evolved for 1 simulated yr, requiring nearly six million 5 s time steps.

4. GRAVITY WAVE GENERATION AND PROPAGATION

Internal gravity waves are self-consistently generated at the convective-radiative interface and subsequently propagate into the stable radiative interior, where they are either dissipated (via radiative damping, critical layer absorption, or wave breaking) or set up standing waves. The wave spectrum has been discussed in detail in Rogers & Glatzmaier (2005) and we discuss it here only as a brief introduction. Figure 1 shows the power spectrum of waves at the convective-radiative interface after approximately 10 months of integration.[1] Power is broadly distributed in frequency and horizontal wavenumber at the interface. This spectrum is *not* concentrated at the convective turnover frequency, showing significant energy both well below that frequency (down to our minimum calculated frequency of 1 μHz) and well above. Relative to analytic models this means that momentum deposition in our model occurs over a wider range of depths.

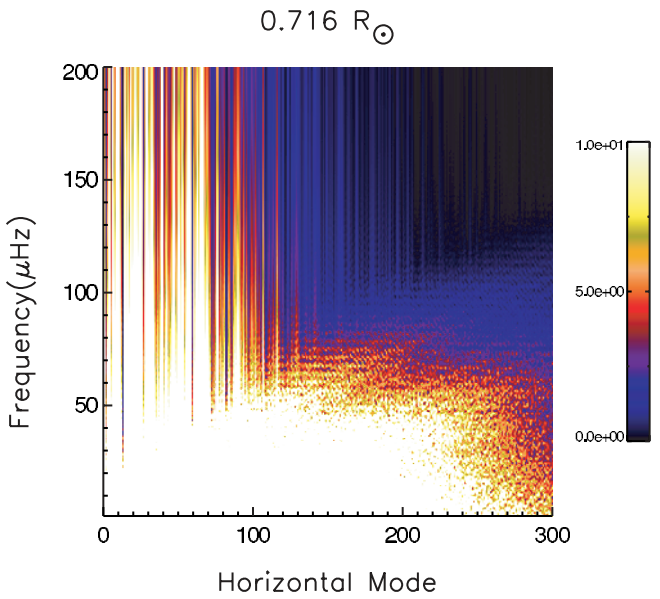

FIG. 1.—Power spectrum (cm^2 s^{-2}) of gravity waves just beneath the convection zone. Energy is broadband in both frequency and wavenumber. Note that any frequency/wavenumber combination with power greater than 10 cm^2 s^{-2} is represented as white.

The downward flux of kinetic energy for horizontal mode $m = 1$ at the convective-radiative interface is compared to the analytically derived flux in KTZ99 (eq. [27] their paper, normalized using their Fig. 2) in Figure 2. We compare the flux at values of frequency divided by the convective turnover frequency because of the different values for turnover frequency achieved in each model.[2] As can be seen in Figure 2, our model predicts significantly lower kinetic energy flux at $m = 1$, but that flux is distributed rather uniformly in frequency relative to the large frequency drop assumed in KTZ99. An integration over all frequencies and wavenumbers yields a vertical kinetic energy flux similar to that estimated previously in several works, namely $F_{\rm waves} = F_T M$, where $F_{\rm waves}$ is the vertical kinetic energy flux at the base of the convection zone, F_T is the total flux through the system, and M is the Mach number for the convective motions.

5. CONVECTION ZONE AND TACHOCLINE

5.1. *Angular Velocity Variations*

Helioseismic observations indicate that, in the equatorial plane, the convection zone spins faster than the radiative interior.

[1] Note that this spectrum is slightly different than that shown in Rogers & Glatzmaier (2005) because of the imposed differential rotation at the tachocline.

[2] Because of our increased thermal diffusivity, the convective velocities here are larger, leading to a convective turnover frequency of around 10 μHz, while KTZ99 assume convective turnover frequencies of around 0.1 μHz.

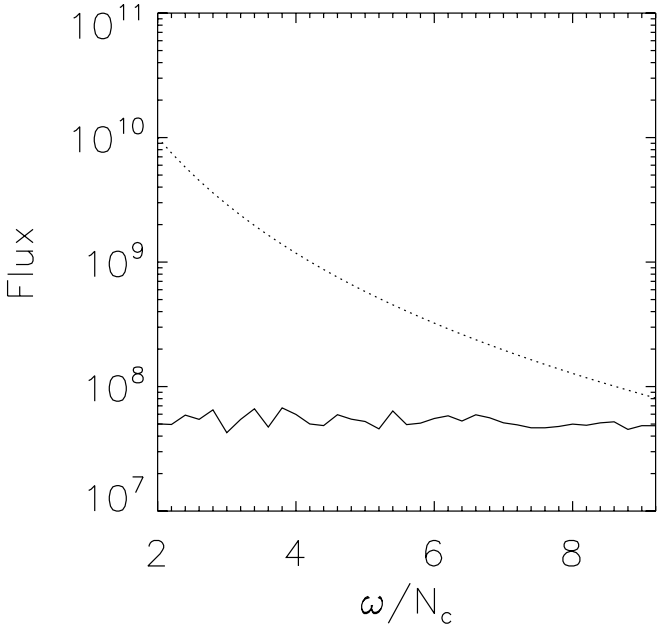

FIG. 2.—Energy flux (ergs cm^{-2} s^{-1}) beneath the convection zone for the numerical simulation presented here (*solid line*) and from analytic predictions (*dotted line*; KTZ99). The flux is plotted as a function of frequency ω divided by the typical convective turnover frequency N_c for a more direct comparison. The numerical simulation yields a much lower amplitude flux which is distributed rather uniformly in frequency relative to that predicted analytically. The numerical spectrum is not peaked at the convective turnover time. Note that while our numerical simulation produces frequencies 10 times smaller than the convective turnover frequency, we do not plot them here because the KTZ99 model does not generate them.

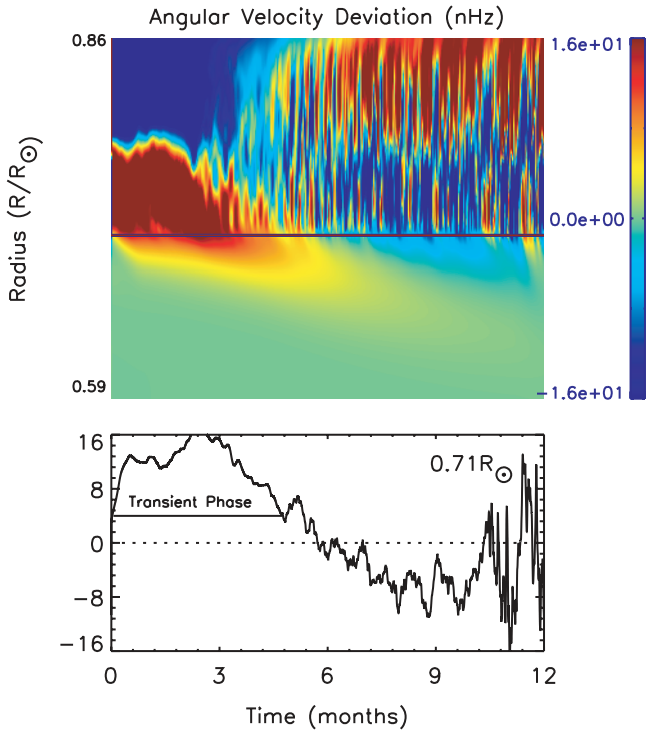

FIG. 3.—Angular velocity variations. *Top*: Angular velocity variations relative to the prescribed solar profile as a function of time and radius. Red represents prograde motion while blue represents retrograde motion. The black line represents the convective-radiative interface. Variations are shown in nHz. *Bottom*: Angular velocity variation as a function of time at the convective-radiative interface. The dotted line represents zero fluctuation about the mean. Note that the first ~4 months are an initial adjustment stage.

The maintenance of differential rotation within the equatorial plane of the convection zone is a three-dimensional (3D) process involving the transport of angular momentum in both radius and latitude, and the Coriolis forces resulting from axisymmetric meridional circulation. Since our 2D geometry captures only the transport in radius, we cannot expect to achieve a realistic differential rotation profile with the 2D model. Therefore, we impose the observed equatorial angular velocity as a function of radius in our model. As mentioned above, the background angular velocity is set to a constant 465 nHz in the convection zone and to a constant 435 nHz in the radiation zone; we prescribe a smooth fit between these two values through the thin tachocline shear layer. The resulting gravity-wave spectrum and angular momentum transport is then investigated.

The time series of angular velocity $\Omega'(r, t)$ relative to the prescribed background angular velocity $\Omega(r)$ for this model is shown in Figure 3 over 1 simulated year. As seen in this figure, angular velocity in the convection zone is initially prograde, relative to the prescribed $\Omega(r)$, in the lower part of the convection zone and retrograde motion in the upper part. However, after this initial adjustment period, angular velocity becomes very time dependent and is predominantly retrograde in the lower part of the convection zone and prograde in the upper part. This profile persists for the last 8 months of integration, and is expected given the density stratification and rotation of the solar interior. Within the convection zone vorticity is locally generated by plumes rising and sinking from the boundaries. The angular momentum transport from this process and the resulting angular velocity is ultimately dictated by the density stratification (G. A. Glatzmaier et al. 2007, in preparation). The density stratification in the Sun, with smaller density scale height in the outer convection zone than in the inner convection zone, leads to predominantly retrograde

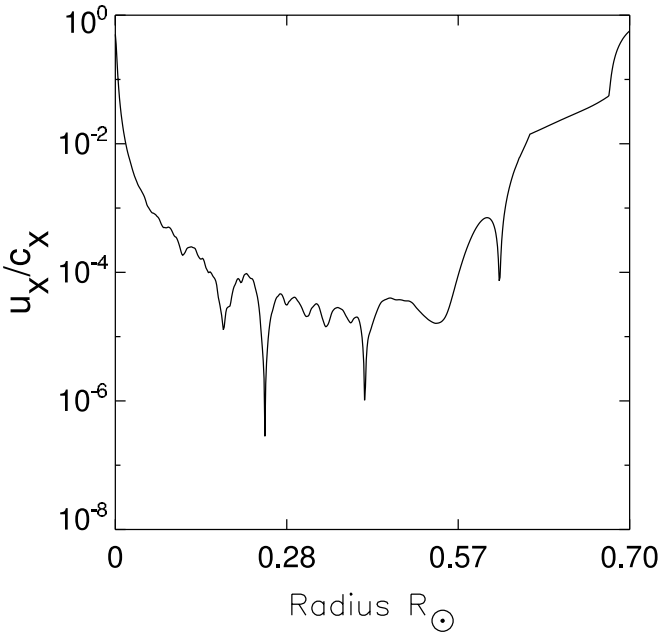

FIG. 4.—Ratio of fluid velocity to the phase velocity (for a typical frequency and wavenumber), also known as the Froude number, a measure of the nonlinearity of the waves. This figure shows that motions are clearly nonlinear in the tachocline and the core.

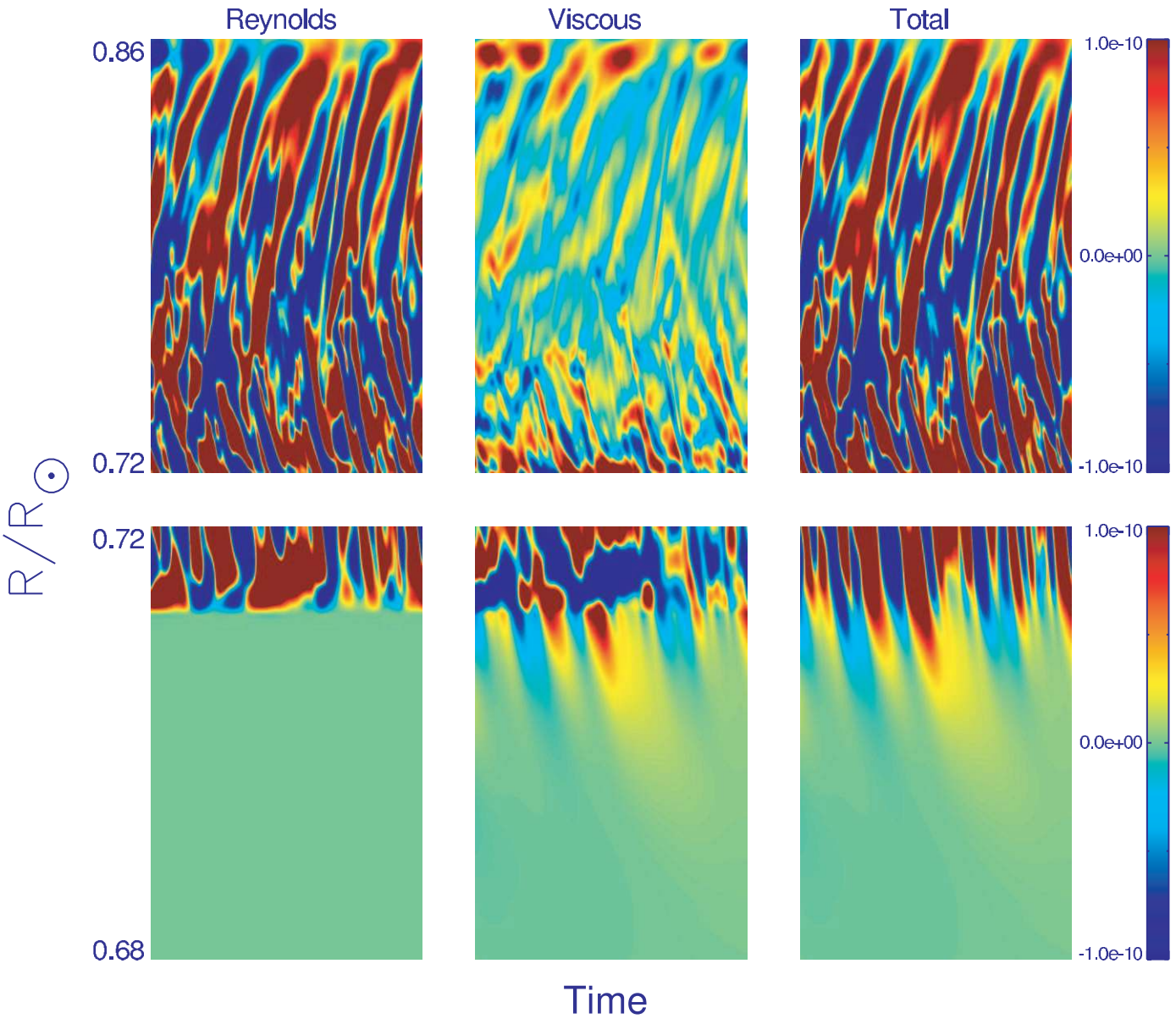

FIG. 5.—Convergence of the mean Reynolds stress, viscous stress, and the sum $\partial\overline{U}/\partial t$, over a 5 day period in both the convection zone (*top*) and overshoot region (*bottom*; enlarged in radius by a factor of 3.5 relative to the top row). A semiperiodic oscillation is seen both in the convection zone and overshoot region. This oscillation causes an oscillation in the amplitude (but not direction) of the mean zonal flow seen in Fig. 3. Note that any mean Reynolds stress, viscous stress, or sum that has a magnitude greater than 10^{-10} cm s^{-2} is represented as red. Similarly, any value with a magnitude less than -10^{-10} cm s^{-2} is represented as blue. Therefore, the color scale does not distinguish the very small differences between the highest prograde and retrograde amplitudes.

flow at the base of the convection zone and prograde motion near the top. This convective process dictates the nature of the motions generated at the convective-radiative interface and subsequently in the tachocline.

Intermittently, prograde motion from the top of the convection zone will extend to the base of the convection zone and overshoot into the tachocline. The angular velocity variations produced by these motions vary in amplitude between ± 15 nHz, slightly larger than the amplitudes of the observed 1.3 yr oscillation[3] (Howe et al. 2001). Figure 3 (*top*) clearly shows that the angular velocity of the tachocline mimics the behavior in the lower part of the convection zone; when the lower convection zone is prograde, the tachocline is prograde and vice versa. This is an indication that the behavior of the tachocline is dictated by convection zone dynamics, rather than by gravity waves (see below).

In the overshoot region fluid motions are strongly nonlinear (Rogers & Glatzmaier 2005). Figure 4 shows the ratio of the horizontal fluid velocity to the horizontal phase speed (the Froude number) for a typical frequency and wavenumber (20 μHz, $m = 10$); this provides a measure of the nonlinearity of waves. For linear waves $u_x/c_x \ll 1$. However, as is clearly seen in Figure 4, this criterion does not hold just below the convection zone. While only one ratio is shown as a function of radius, this can vary by an order of magnitude depending on the choice of frequency and wavenumber.[4] However, using reasonable values for frequency and wavenumber, the smallest value of this ratio just

[3] These amplitudes are similar to those found in Talon et al. (2002). This similarity is likely due to the fact that the integrated energy transferred to the stable region is similar in the two models, although the spectrum is different.

[4] For larger (smaller) values of the horizontal wave mode number this ratio is larger (smaller). Similarly, for larger (smaller) frequencies this ratio is smaller (larger).

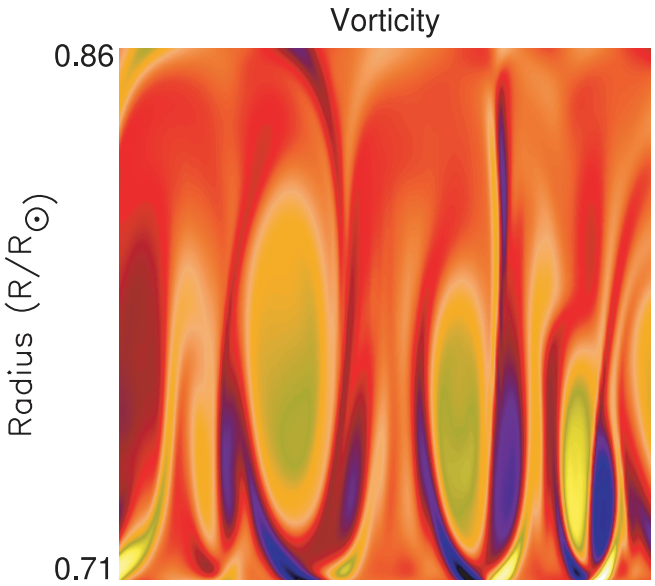

FIG. 6.—Zoom in of vorticity in the convection zone in the equatorial plane viewed from the northern hemisphere. Large cells span the bulk of the convection zone with counterrotating cells beneath due to the deflection of descending plumes as they encounter the stiff radiative region. Red and green are counterclockwise rotating eddies, and blue is clockwise.

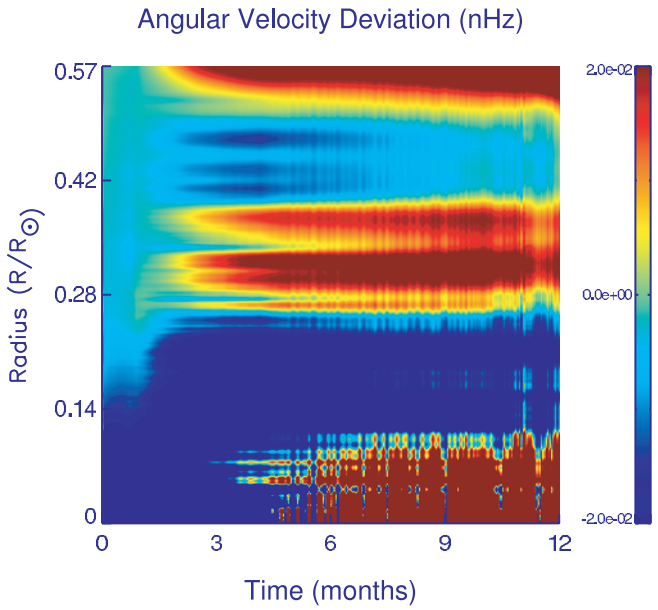

FIG. 7.—Angular velocity variations in the deep interior. Banded radial differential rotation is seen here. The deviations in the core are 2–3 orders of magnitude larger than those in the bulk of the radiative interior. There appears to be a link between deviations in the core and those in the tachocline (see Fig. 3).

below the convection zone is 0.1, still far from meeting the linearity criterion above. Furthermore, it is clear in this figure that linearization may not be justified in the solar core either, as suggested by Press (1981).

The typical properties of a wave-driven oscillation are missing in the tachocline in Figure 3 (*top*). There is no sign of a double-peaked shear layer with retrograde motion underlying the prograde (or vice versa). The disturbances in angular velocity do not move upward (toward the source) in time, and the motions in this region do not have different timescales than their source (the convection zone). There appears to be no QBO-like oscillation.

5.2. *Reynolds and Viscous Stresses*

The mean zonal flow is determined by a balance between viscous and Reynolds stresses (as seen in eq. [1]). In order to better understand the angular velocity profile in time (as shown in Fig. 3) we examine the sources of that balance. Figure 5 shows the horizontally averaged convergence of Reynolds stress (first term on the right hand side of eq. [1], but now in cylindrical coordinates), the viscous stress (second term on the right hand side of eq. [1], in cylindrical coordinates), and the sum of these (the time rate of change of the mean zonal flow $\overline{U}$) in both the convection zone and overshoot region over 5 days.

In the model's convection zone, the Reynolds stresses are much larger than the viscous stresses. The pattern of Reynolds stress convergence has a semiperiodic behavior with disturbances propagating up and down from a radius near 1/3 d_{cz} (d_{cz} is the convection zone depth). When positive (i.e., prograde) Reynolds stress convergence moves upward from this radius a negative value moves downward and vice versa. This process reverses with a frequency similar to the convective turnover frequency, roughly twice the solar rotation rate. This oscillatory behavior is observed in our simulations only when we include a radiative region beneath the convection zone; we do not see it when we impose an impermeable lower boundary on the convection zone. Note also that this radius of 1/3 d_{cz} is approximately where $\boldsymbol{v}_\theta$ for the large eddies changes sign, and below which smaller, counterrotating cells exist. Figure 6 shows a zoomed-in region of the convection zone, displaying the vorticity within a few convective cells (red and green are counterclockwise rotating eddies, and blue are clockwise). Beneath the large cells spanning most of the convection zone is counterrotating fluid that is driven by the retrograde tilted, downwelling plumes penetrating slightly into the stable overshoot region. As a plume rebounds it is diverted laterally exciting counterrotating eddies adjacent to it. It remains to be seen how these counterrotating cells affect tachocline dynamics in a 3D simulation.

Now consider the overshoot region in our model. Regions with positive or negative Reynolds stress convergence in the lower convection zone correspond to the same signed disturbances in the overshoot region. These disturbances have a slight tendency to propagate downward, i.e., away from their source in the convection zone. When viscous terms are added (which in the overshoot region have magnitudes similar to the Reynolds stress terms), disturbances clearly propagate away from the convection zone (Fig. 5). This motion away from the convection zone is also seen in Figure 3, and is due to diffusion away from the source.[5]

A semiperiodic oscillation in $\partial\overline{U}/\partial t$ is observed both within the convection zone as well as in the overshoot region (Fig. 5). However, this oscillation mainly affects the amplitude of $\overline{U}$, usually not changing its direction (Fig. 3). This is because retrograde motions have a (very) slightly larger amplitude than prograde motions. The asymmetry between prograde and retrograde amplitudes in the overshoot region could arise from asymmetrical driving by the convection zone or by wave damping in the presence of differential rotation. There are several arguments that favor asymmetric driving by the convection zone. First, an oscillation in the sign of $\partial\overline{U}/\partial t$ is observed within the convection zone, without a corresponding sign oscillation in $\overline{U}$. Second, the radial differential profile set up in the convection zone favors retrograde motion near the base of the convection. Finally, mean

[5] Even if diffusion were neglected the disturbances do not move upward as in the QBO.

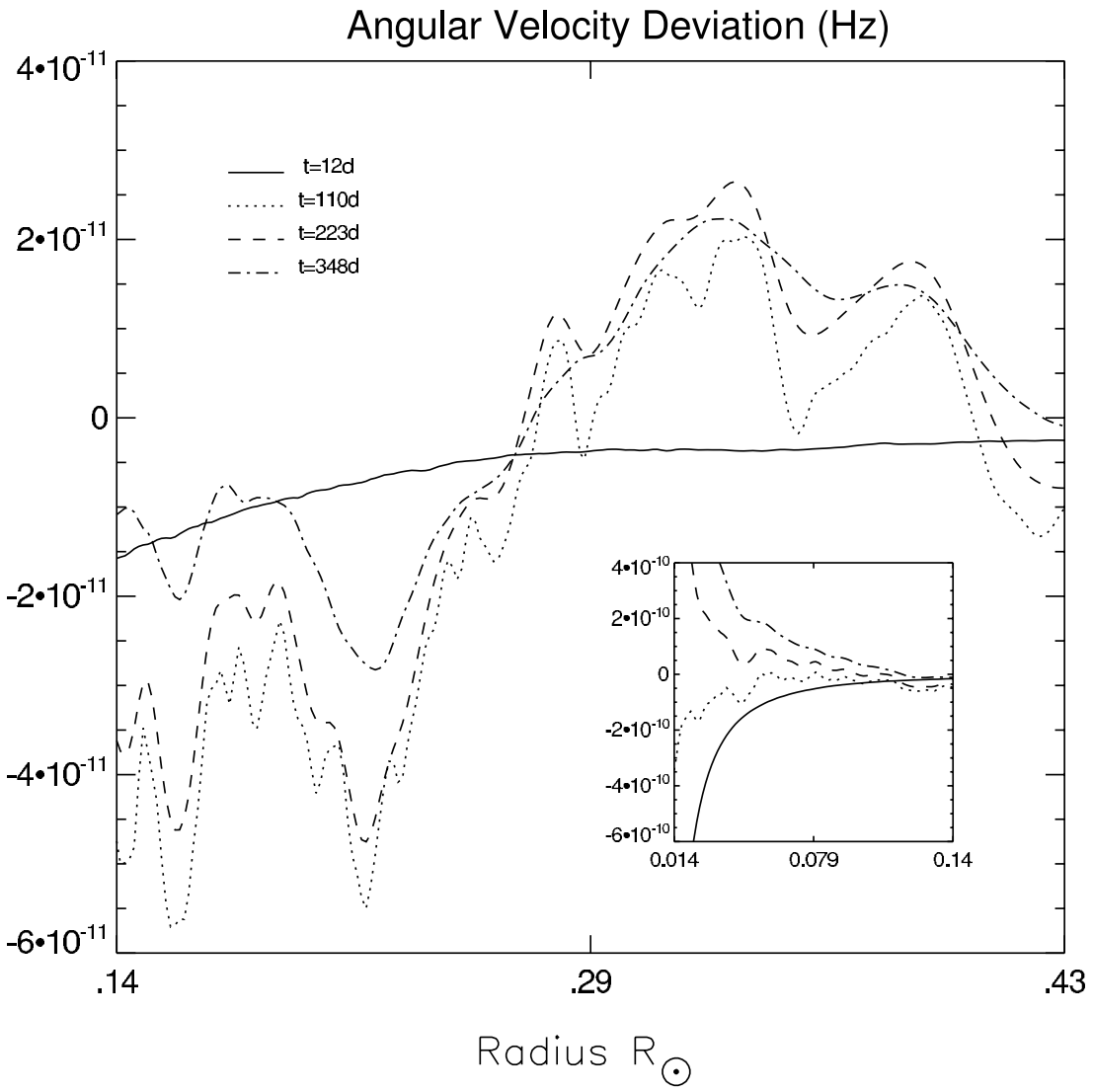

FIG. 8.— Time evolution of angular velocity variations. Some indication of a reversal is underway in the bulk of the radiative interior between 223 days and 348 days. In the core there was clearly a reversal, which Fig. 7 tells us was around 130 days.

Reynolds stresses in the overshoot region are visibly linked to similarly signed stresses in the convection zone, i.e., they do not have different magnitudes or periods that one would expect if they were due to differential wave damping.[6] For these reasons, and because there is no physical justification for symmetric driving, we conclude that prograde and retrograde motions in the overshoot region are asymmetrically driven by the convection zone.

There is clearly a strong correlation between Reynolds stresses (Fig. 5) and mean angular velocity (Fig. 3) at the base of the convection zone and in the overshoot region. This connection provides a convincing argument that angular velocity disturbances in the overshoot region and tachocline (at least the top of the tachocline) are driven by convective processes. Furthermore, the absence of the main properties of a wave driven oscillation (motion toward the generation site in time, timescales different than the forcing timescales, and a double-peaked shear layer) indicate that these processes are not dominant in the overshoot region. Given the spatially and temporally dependent filter on waves excited by these overshooting motions, it is unlikely that a coherent double-peaked shear layer could ever develop in the shallow region just below the convection zone, although this process may develop deeper down (see §§ 6 and 7). It appears that overshooting plumes themselves transport angular momentum in a way that is distinct from the nonlinear interaction of low-amplitude waves that produces a shear layer oscillation. These plumes are buoyantly braked and radiatively damped, and their nonlinearity allows for mode-mode transfer which affects the damping rate. The transport is time dependent and depends critically on convection zone dynamics. Therefore, it may be quite difficult to quantitatively predict the behavior in this region without more realistic 3D simulations. However, these 2D simulations do suggest that the tachocline dynamics cannot be characterized as a nonlinear interaction of infinitesimal waves.

6. THE DEEP INTERIOR AND CORE

A banded radial differential rotation profile is observed deep within the radiative interior (Fig. 7). However, the amplitude of the angular velocity variation is extremely low (0.02 nHz) relative to what it is in the convection zone and overshoot region. This radial shear grows in time (Fig. 8) due to wave-wave interactions which enforce shear. However, there is some indication that the

[6] We have also run a model with no imposed differential rotation which produces the same asymmetry, further corroborating our conclusion.

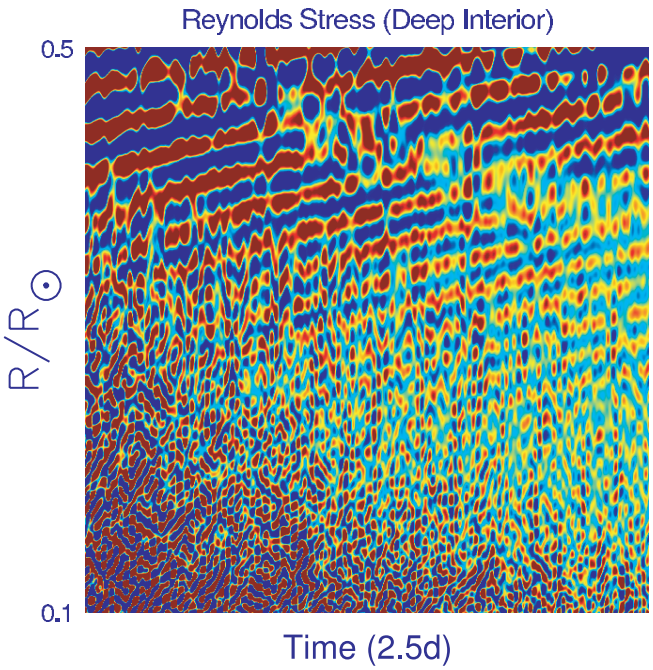

FIG. 9.—Convergence of the mean Reynolds stress in the bulk of the radiative interior (blue represents negative, red positive values). Disturbances move upward in time as expected from the nonlinear interaction of low-amplitude waves. Significant interference is seen at smaller radii, probably due to the interaction of inward propagating and reflected waves.

growth is slowing and possibly reversing (Fig. 8) due to increased viscous diffusion as angular velocity gradients increase; however, we have not run the model long enough for a conclusive reversal. The banded differential rotation is due to the broad spectrum of frequencies generated and their *continual* deposition of angular momentum due to radiative diffusion as they propagate. Banded differential rotation in the Sun's radiative interior has not been inferred from helioseismology, possibly because the amplitude is too low, or because these small-amplitude disturbances are easily neutralized in 3D. In the core of our model the amplitude of the angular velocity variation is 2–3 orders of magnitude higher than in the bulk of the radiative interior. This indicates that angular momentum transport from waves to zonal flow is more efficient in the core, which could be due to a number of factors, including wave breaking, critical layers (where the phase speed of the wave approaches the mean rotation rate), or inefficient reflection as the wave frequency approaches the Brunt-Väisälä frequency. Angular velocity near the center is also enhanced because of geometry. That is, very little angular momentum deposition is needed at small radii to produce large changes in the angular velocity there. However, we find that angular momentum deposition in the central region is more than a geometrical effect.

Maxima in the convergence of the mean Reynolds stress deep within the radiative interior (but a significant distance below the overshoot region) propagate upward (Fig. 9) like a QBO, as expected from the nonlinear interaction of low-amplitude waves (see § 2). In addition, significant interference is seen in the lower radiation zone, which likely comes from the interaction of inward propagating and outward-reflected waves. While we have not observed a complete reversal of the angular velocity in the bulk of the radiative region, there is some evidence that one is underway (Fig. 8).

The growth timescale for a wave-driven, double-peaked shear layer is inversely proportional to the total kinetic energy flux in waves and to the thermal diffusivity (Plumb 1977). In our simulation the total flux and the thermal diffusivity are larger in the overshoot region than they are in the deep radiative interior. Therefore, if a double-peaked shear layer could develop in the overshoot region it would do so in a shorter time than such a shear in the deep interior (i.e., in a shorter time than we have simulated). However, a shear in the overshoot region does not develop, not because of an insufficient integration time, but because the angular momentum transport by overshooting plumes dominates this region. In the core the mean angular velocity switches from retrograde to prograde at nearly the same time as the tachocline switches from prograde to retrograde. This suggests that the angular velocity of the core may be linked to the angular velocity of the tachocline, and hence of the convection zone. The link between tachocline angular velocity and that of the core due to selective filtering has been elucidated previously in Talon et al. (2002). Here we make the link between the tachocline and the convection zone, and propose that a self-consistent study of differential rotation in the Sun must not treat the radiative and convective regions separately.

7. DISCUSSION

Despite some similarity between the convective-radiative interface in the Sun and the Earth's tropopause, there are several obvious differences. In the Sun, convection is constantly driving gravity waves everywhere below the overshoot region, whereas the generation of large amplitude gravity waves in the Earth's atmosphere is intermittent in time and space. Solar gravity waves travel down into a converging region of increasing density, whereas in the Earth's atmosphere waves travel up into an expanding region of decreasing density. Furthermore, previous numerical simulations of convective penetration in a stratified atmosphere demonstrate a remarkable difference between penetration into an overlying stable region and penetration into an underlying stable region (Hurlburt et al. 1986). Penetration into an underlying stable region is characterized by thin localized downflows, whereas penetration into an overlying stable region is characterized by larger scale broad upflows. This asymmetry allows descending plumes to travel farther into an underlying stable region than ascending motions travel into an overlying stable region. Therefore, it is likely that penetrative convection plays a more crucial role at the base of the solar convection zone than it does at the Earth's tropopause. These differences can have profound effects on the role of overshoot, and hence on the scale, frequency, and amplitude of the waves generated, and so on the angular momentum transport by these waves.

Numerical simulations (Wedi & Smolarkiewicz 2006) of the Plumb-McEwan laboratory experiment attempting to reproduce the QBO have shown that the type and period of an oscillation in the differential rotation profile depend sensitively on the forcing. In particular, it is found that random forcing rarely produces a periodic oscillation. Given the turbulent nature of the Sun, it is likely that the forcing is fairly random.

For reasons stated above, it is unlikely that there is a QBO-like oscillation associated with the solar tachocline where the region is dominated by convective overshoot. However, QBO-like oscillations may occur in stars with radiative envelopes because of the inefficiency of overshoot into an overlying stable region and because of a more similar geometry.

8. CONCLUSIONS

We have presented self-consistent numerical simulations of convective overshoot and gravity wave generation, and the angular momentum transport by these processes in a 2D model of

the dynamics in the solar equatorial plane. We find that angular velocity variations in the tachocline are driven by angular momentum transported by overshooting plumes rather than the nonlinear interaction of low-amplitude waves. These overshooting plumes are strongly nonlinear disturbances, which cannot be accurately represented as an increased flux of low-amplitude waves. We observe a semiperiodic oscillation in amplitude, but not in direction, of the mean flow in the tachocline because of an asymmetry in the driving of prograde and retrograde motions. No QBO-like oscillation is seen in our simulated tachocline. Since we find that linear gravity waves are not dominant in the tachocline, it is unlikely that they are responsible for the 1.3 yr oscillation or the 11 yr solar cycle. It is no surprise that overshooting motions play a dominant role in the tachocline, and we expect these results will persist in three-dimensions.

In the deep radiative interior the continual deposition of angular momentum by the nonlinear interaction of gravity waves produces a radially banded differential rotation. Our 2D simulation does show indications of a low-amplitude QBO-like oscillation well below the tachocline. However, it remains to be seen whether this pattern persists in 3D, considering its very low amplitude.

In the model's core, the amplitude of the differential rotation (i.e., angular velocity relative to the solar rotation rate) is about 2 orders of magnitude larger than that in the bulk of the radiative region and similar to the magnitude within the convection zone. We observe retrograde motion in the core reversing to prograde motion in step with the counterreversal (prograde to retrograde) at the tachocline. When there is predominantly prograde flow at the base of the convection zone it selectively filters out prograde propagating gravity waves, allowing predominantly retrograde waves to propagate to the core where they deposit their (negative) angular momentum, and vice versa (Talon et al. 2002). Like previous results our simulations therefore suggest that the angular velocity variations in the solar core are linked to those in the tachocline. However, unlike previous results we show here that the variations in the tachocline are driven by convective overshooting, therefore linking core rotation to convective motions.

Unlike one dimensional parameterized models that make huge simplifications, here we have calculated a 2D model that self-consistently generates the waves and accurately calculates the nonlinear interaction responsible for angular momentum transport. However, it is evident that the nature of angular momentum transport by waves depends sensitively on the driving of the waves and on the angular velocity profile those waves travel through. The driving of waves will likely depend on the vigor of the fluid motion, i.e., the Rayleigh and Reynolds numbers, and on the dimensionality of the problem. It is likely that the frequency and wavenumber spectra of the excited gravity waves would be broadly distributed in a 3D turbulent simulation because of the increased degrees of freedom. As mentioned above, a broad spectrum means a larger range in depth over which angular momentum is transported. The angular velocity profile just below the convection zone is likely determined by convective overshoot, which also depends on the dimensionality of the problem. Because of these dependencies, description of the fluid motion in the radiative interior is a very complex issue that depends on convective turbulence, overshoot, and nonlinear wave interactions in three dimensions.

We thank J. Christensen-Dalsgaard, P. Garaud, D. Gough, C. Jones, K. MacGregor, and M. Metchnik for helpful discussions and guidance. T. R. would like to thank the National Physical Science Consortium for a graduate student fellowship and the Institute of Astronomy, Cambridge University for a travel grant. Support has also been provided by the DOE SciDAC program DE-FC02-01ER41176, the NASA Solar and Heliospheric Program SHP04-0022-0123 and the University of California at Santa Cruz Institute of Geophysics and Planetary Physics. Computing resources were provided by NAS at NASA Ames and by the NSF MRI grant AST 00-79757.

REFERENCES

Baldwin, M. P., et al. 2001, Geophys. Res. Lett., 39, 179
Garcia-Lopez, R. J., & Spruit, H. 1991, ApJ, 377, 268
Goldreich, P., Murray, N., & Kumar, P. 1994, ApJ, 424, 466
Goldreich, P., & Nicholson, P. D. 1989, ApJ, 342, 1079
Gough, D. O., & McIntyre, M. E. 1998, Nature, 394, 755
Holton, J. R. 1994, An Introduction to Dynamic Meteorology (4th edition; New York: Academic)
Holton, J. R., & Lindzen, R. S. 1972, J. Atmos. Sci., 29, 1076
Howe, R., Christensen-Dalsgaard, J., Hill, F., Komm, R. W., Larsen, R. M., Schou, J., Thompson, M. J., & Toomre, J. 2001, Science, 287, 2456
Hurlburt, N. E., Toomre, J. , & Massaguer, J. M. 1986, ApJ, 311, 563
Kim, E., & MacGregor, K. B. 2001, ApJ, 556, L117
Kumar, P., & Quataert, E. 1997, ApJ, 475, L143
Kumar, P., Talon, S., & Zahn, J. P. 1999, ApJ, 520, 859 (KTZ99)
Leovy, C. B., Friedson, A. J., & Orton, G. S. 1991, Nature, 354, 380
Lindzen, R. S. 1990, Dynamics in Atmospheric Physics (Cambridge: Cambridge Univ. Press)
Lindzen, R. S., & Holton, J. R. 1968, J. Atmos. Sci., 25, 1095
Montalban, J. 1994, A&A, 281, 421
Plumb, R. A. 1977, J. Atmos. Sci., 34, 1847
Plumb, R. A., & McEwan, A. D. 1978, J. Atmos. Sci., 35, 1827
Press, W. H. 1981, ApJ, 245, 286
Ringot, O. 1998, A&A, 335, L89
Rogers, T. M., & Glatzmaier, G. A. 2005, MNRAS, 364, 1135
Schatzman, E. 1993, A&A, 279, 431
Talon, S., & Charbonnel, C. 2005, A&A, 440, 981
Talon, S., Kumar, P., & Zahn, J. P. 2002, ApJ, 574, L175
Terquem, C., Papaloizou, J. C. B., Nelson, R. P., & Lin, D. N. C. 1998, ApJ, 502, 788
Wedi, N. P., & Smolarkiewicz, P. K. 2006, J. Atmos. Sci., in press
Zahn, J. P. 1975, A&A, 41, 329
Zahn, J. P., Talon, S., & Matias, J. 1997, A&A, 322, 320